Post-print of: Thermochimica Acta, Volume 526, Issues 1–2, 10 November 2011, Pages 222–228

Influence of Al2O3 reinforcement on precipitation kinetic of Cu–Cr nanocomposite

S. Sheibani (a), A. Ataie (a), S. Heshmati-Manesh (a), A. Caballero (b), J.M. Criado (b)

(a) School of Metallurgy and Materials Engineering, University of Tehran, Tehran, Iran

(b) Instituto de Ciencia de Materiales de Sevilla, Departamento de Química Inorgánica, CSIC – Universidad de Sevilla, Américo Vespucio 49 Sevilla, Spain

Abstract

In this paper, the kinetic of precipitation process in mechanically alloyed Cu-1 wt.% Cr and Cu-1 wt.% Cr/3 wt.% Al2O3 solid solution was compared using differential scanning calorimetry (DSC), X-ray diffraction (XRD) and transmission electron microscopy (TEM). The ageing kinetics in Cu–Cr and Cu–Cr/Al2O3 can be described using Johnson–Mehl–Avrami (JMA) and Sestak–Berggren (SB) models, respectively. These different behaviors have been discussed in details. It was found that in presence of Al2O3 reinforcement, the ageing activation energy is decreased and the overall ageing process is accelerated. This behavior is probably due to higher dislocation density previously obtained during ball milling and Al2O3–Cu interface. TEM observations confirm that Al2O3–Cu interface and structural defects act as a primary and secondary nucleation sites, respectively.

Keywords

Ageing; Cu–Cr/Al2O3; Mechanical alloying; Nanocomposite; Precipitation kinetics

1. Introduction

Copper matrix composites reinforced with metallic precipitates, i.e. in situ composites, or ceramic particles, like Al2O3, ZrO2 or TiC [1], [2] and [3], have received a great deal of attention in recent years. These composites possess advantageous properties, in particular, high electrical and thermal conductivity and good mechanical properties. Thus, they are very attractive materials for various industries [4]. Cu–Cr system is an in situ composite resulting from decomposition of the supersaturated Cu–Cr solid solution. In fact, by ageing treatment of solid solution, the Cr precipitated through nucleation and growth mechanism in the Cu matrix [5], [6] and [7]. Different methods have been used to produce Cu–Cr solid solution. Among them, mechanical alloying has attracted a lot of attention in recent years. Extension of Cr solubility in Cu during mechanical alloying

and the effect of Al2O3 nano-particles on the Cr solubility have already been investigated [8] and [9].

On the other hand, thermal analysis methods such as differential thermal analysis (DTA) or differential scanning calorimetry (DSC) have been extensively used to study the kinetic analysis of solid state processes. These techniques measure the temperatures and heat flows associated with transformation in materials. Such measurements provide quantitative and qualitative information about the transformation in endothermic or exothermic processes [10], [11], [12] and [13].

Many investigations have been devoted to the study of the solid state ageing behavior of Cu–Cr in situ composite in the aspects of microstructure, mechanical and electrical properties [5], [6], [7], [14], [15], [16], [17], [18], [19] and [20]. Kinetics of ageing or Cr precipitation has not yet been thoroughly studied using thermal analysis. Specially, the influence of ceramic reinforcements on the ageing behavior of this system, which has not been studied yet, seems interesting. The aim of this study is a quantitative analysis of the non-isothermal heat treatment of Cu–Cr solid solution in order to obtain the kinetic parameters characterizing the Cr precipitation process in Cu matrix. The effect of the Al2O3 nano-particle on the kinetic of precipitation is also studied. It is very important to determine reliable kinetic parameters enabling control of the precipitation process under defined conditions. Knowledge of both the mechanism and the kinetics of ageing make it possible to predict the characteristics of precipitates resulting from different ageing conditions.

2. Theory

The rate of the process dα/dt is proportional to the measured specific heat flow Φ, normalized per sample mass (W/g) [10]:

$$\frac{d\alpha}{dt} = \frac{\phi}{\Delta H} \qquad (1)$$

where t is time and ΔH corresponds to the total enthalpy change associated with the precipitation process. It could be noticed that ΔH corresponds to the total peak area of the DSC curve. The fractional conversion α can be easily obtained by partial integration of DSC curve [10]:

$$\alpha = \frac{1}{\Delta H \beta} \int_{T_0}^{T} \phi dT \qquad (2)$$

where β is the heating rate and T is the absolute temperature. Also, T0 corresponds to the beginning temperature of the baseline approximation when the measured specific heat flow is equal to zero. Eq. (2) is valid under linear heating conditions. On the other hand, the rate of the kinetic process can be expressed as a product of temperature dependent rate constant k(T) and a dependent kinetic model function f(α) [10]:

$$\frac{d\alpha}{dt} = k(T) f(\alpha) \quad (3)$$

f(α) functions used for description of nucleation and growth processes most frequently, are summarized in Table 1.

The rate constant in Eq. (3) follows Arrhenius form [10]:

$$k(T) = A \exp\left(\frac{-E}{RT}\right) \quad (4)$$

where A is the pre-exponential factor, R is the gas constant and E is the activation energy which should not depend on T and α. Combining Eqs. (1), (3) and (4) the following equation is obtained:

$$\phi = \Delta H f(\alpha) A \exp\left(\frac{-E}{RT}\right) \quad (5)$$

The aim of a kinetic analysis is to find the best kinetic model providing the calculation of reliable kinetic parameters A and E. Calculation of E is based on a multiple-scan method in which several measurements performed at different heating rates. This value has been determined from the isoconversional Kissinger equation [26]:

$$\ln\left(\frac{\beta}{T_p^2}\right) = -\frac{E}{RT_p} + \ln\left(\frac{RA}{E}\right) \quad (6)$$

where Tp is the peak temperature. Therefore, E and A can be obtained from the plot $\ln(T_p^2/\beta)$ vs. $1/T_p$. It is noteworthy to point out that although the Kissinger equation was developed by assuming "n order" kinetic models, it was later demonstrated [27] and [28] that it applies for any other kinetic models like diffusion controlled reaction or Avrami–Erofeev kinetic models. It has been also reported that the error of the activation energy determined from the Kissinger method [27] and [29] is very small for values of E/RT > 5. However, the use of this method implies to assume that the activation energy remains constant all over the process, what is not evident a priory and therefore, additional kinetic information would be required in order to check if the activation energy remains constant all over the α range [29]. It has been shown [11], [12] and [13] that the y(α) and z(α) functions obtained at different heating rates are overlapping only if the real activation energy has been used for obtaining these curves. Thus, the calculation of these functions from the DSC curves obtained at different heating rates by using the Kissinger activation energy would be a proper criterion for discerning if the activation energy is independent of the reacted fraction.

The y(α) and z(α) functions can be easily obtained by a simple transformation of experimental DSC data. For practical reasons the y(α) and z(α) functions are normalized within (0,1) interval. In non-isothermal conditions these functions are defined as [11], [12] and [13]:

$$y(\alpha) = \phi \exp\left(\frac{E}{RT}\right) \quad (7a)$$

$$z(\alpha) = \phi T^2 \quad (7b)$$

Both the y(α) and z(α) dependences and properties can be used to guide the choice of a kinetic model [11], [12] and [13]. These functions exhibit maxima at αM and α_p^{∞}, respectively. If the α_p^{∞} lies within the interval $0.62 < \alpha_p^{\infty} < 0.64$ then the DSC data can probably be described within the JMA model. The value of $\alpha_p^{\infty} = 0.632$ is a characteristic fingerprint of the JMA model. On the other hand, if $\alpha_p^{\infty} < 0.62$ then the SB empirical model provides a more satisfactory description of the experimental DSC data [11], [12] and [13]. The kinetic exponent n for JMA model can be calculated using the following equation [12]:

$$n = \frac{1}{1 + \ln(1 - \alpha_M)} \quad (8)$$

Also, the ratio of the kinetic exponents M/N for SB model can be calculated using the following equation [12]:

$$\frac{M}{N} = \frac{\alpha_M}{1 - \alpha_M} \quad (9)$$

By substituting SB equation in Eq. (5), the following form may be written:

$$\ln\left[\phi \exp\left(\frac{E}{RT}\right)\right] = \ln(\Delta HA) + N \ln[\alpha^{M/N}(1 - \alpha)] \quad (10)$$

The kinetic parameter N is then calculated from the slope of the linear dependence of ln[ϕexp(E/RT)] versus ln[αM/N(1 − α)] plotted in the interval α ∈ (0.2, 0.8) [12].

Thus, the shape and properties of both y(α) and z(α) functions can be conveniently used to determine the most probable kinetic model. Moreover, the fitting of the whole set of experimental data obtained at different heating rates to single y(α) or z(α) functions would demonstrate that the Kissinger activation energy used for determining the above functions represents the real activation energy of the process.

3. Experimental procedure

Cu-1 wt.% Cr solid solution and Cu-1 wt.% Cr-3 wt.% Al2O3 mixture powders were used for the ageing kinetic measurements. These alloys were prepared through 50 h mechanical alloying in a Fritsch P5 planetary ball mill with ceramic vial (volume of 300 ml) and balls (diameter of 10 and 20 mm) under argon atmosphere. The ball to powder weight ratio and milling speed were 30:1 and 300 rpm, respectively. Details of extended solid solution formation were reported elsewhere [8] and [9].

DSC experiments were performed in a SDT Q600 instrument and argon gas flow of 100 ml/min was applied during the measurement. All experiments were carried out on samples in standard platinum pans, with an empty pan as the standard. The measurements were performed at four different heating rates, i.e. 5, 10, 20 and 40 K/min in the temperature range of 300–1273 K. Then the samples were freely cooled down to room temperature. Once room temperature was reached, the samples are heated a second time at the same heating rate to obtain a baseline. A precise measure of the heat flow can thus be obtained by measuring and integrating the difference between the first and second scans.

The phase identification of the products was carried out by XRD (Philips PW-3710) using Co Kα radiation (λ = 0.17407 nm). The microstructure of the samples was examined by transmission electron microscope TEM (Philips CM200, operated at 200 kV) equipped with an energy dispersive spectrometer (EDS).

4. Results and discussion

The DSC results of Cu–Cr and of Cu–Cr/Al2O3 samples at different heating rates are reported in Fig. 1. These curves, showing similar features, confirmed that both samples undergo the same transformations. All these curves exhibit an exothermic peak, which can be attributed to the decomposition of the solid solution and the precipitation of Cr in Cu matrix. It means that the ageing response of the two materials is relatively similar, differing only by a relative displacement of the peaks. Also, it can be seen in Fig. 1 that, the peak temperature shifts to higher temperatures by increasing the heating rate. This fact shows the kinetic control of the process [30].

The samples were analyzed by XRD before and after the DSC measurements. The XRD patterns of the mechanically alloyed and aged samples for Cu–Cr and Cu–Cr/Al2O3 are shown in Fig. 2. It should be noted that XRD results after DSC measurements at different heating rates did not show an obvious change, and similar results were obtained. Mechanically alloyed sample exhibits broadened peaks, typical of ball milled samples. Meanwhile, the peak width for the aged sample is smaller. Also, a small shift of Cu peak to higher angle after ageing observed in Fig. 2 reveals that Cu lattice parameter has decreased. The reduction of Cu lattice parameter from 0.36189 to 0.36157 nm after ageing may be attributed to the precipitation of the Cr. In fact, Cr solute atoms are driven out of the solid solution and Cu lattice parameter decreased during ageing. Therefore, it was confirmed by XRD results that the exothermic transformation during thermal analysis is related to Cr precipitation. However, the diffraction peak corresponding to Cr was not observed in the XRD patterns, due to its small quantity.

The enthalpy associated with the exothermic peaks was calculated from the integration of the overall DSC curves. These values are summarized in Table 2 and Table 3. The average enthalpies of precipitation in Cu–Cr and Cu–Cr/Al2O3 samples are equal to 14.83 ± 3.57 and 13.78 ± 3.33 J/g, respectively. On the other hand, the theoretical value of Cr precipitation enthalpy for Cu-1 wt.% Cr alloy calculated using CALPAD [26] and

[31] method is approximately 15.8 J/g. It can be observed that, there is a relatively good agreement between the measured and calculated values of the precipitation reaction enthalpy. This also confirms that this stage is due to Cr precipitation in accordance with the XRD analysis.

The value of activation energies of Cu–Cr and Cu–Cr/Al2O3 samples determined by the Kissinger method are 133 ± 5 and 100 ± 3 kJ/mol, respectively. Since Cr precipitation in Cu involves diffusion of Cr, its mobility in the Cu matrix should be the rate-limiting factor in the precipitation process. In fact in Cu–Cr alloys, the precipitation activation energy is closely connected with the activation energy for Cr diffusion [32]. Diffusion activation energy of Cr into undeformed Cu reported in the literature is 220 kJ/mol [33]. It can be found that this is much higher than the value calculated from the Kissinger method. The explanation is that dislocations and lattice defects can form easy diffusion paths for dissolved solute atoms [34]. Therefore, the observed significant decrease in activation energy in both samples compared with undeformed condition can be attributed to an increase in the lattice defects density introduced by mechanical deformation and interfacial energy of supersaturated solution that gave rise to lower activation energy values. Meanwhile, the effect of Al2O3 nano-particles during mechanical alloying on the nanocrystalline solid solution formation in Cu–Cr system was previously investigated [9]. It was reported that, increase of strain or dislocation density brought by the presence of Al2O3 nanoparticles was more significant. Hence, it can be found here that the presence of Al2O3 reinforcement leads to the reduction of Cr precipitation activation energy by about 30 kJ/mol compared to the unreinforced sample. Totally, it can be expected that any modification of the matrix that changes the diffusivity, will change the ageing response of the matrix.

Experimental DSC data can be converted to the z(α) and y(α) functions using Eqs. (7a) and (7b). These two functions, normalized within (0, l) interval, corresponding to Cu–Cr sample are shown in Fig. 3. For better clarity, not all the data points are included in these figures. The shape of the z(α) function is practically invariant with respect to temperature. The validity of the JMA can be easily verified by checking the maximum α_p^{∞} of the z(α) function. α_p^{∞} is a constant and falls into the $0.62 < \alpha_p^{\infty} < 0.64$ range, then the experimental data fits to the JMA model nicely [35]. It has been shown that the applicability of JMA model is restricted by the condition of site saturation which is equivalent to the presumption that the nucleation is completed before the growth process starts. This condition is fulfilled if there is negligible overlap between the nucleation and growth curves [10], [36] and [37]. It should be expected that in the Cu–Cr solid solution sample produced through mechanical alloying, high dislocation and other structural defects density lead to high suitable nucleation sites. Hence, nucleation is probably completed prior to crystal growth. The kinetic exponent for this model calculated using αM (Eq. (8)) together with other parameters are shown in Table 2. These values were used for the kinetic calculation. Experimental data (points) and calculated DSC curves (full lines) are compared in Fig. 1(a) for Cu–Cr sample. It is apparent that the precipitation process can be well described by the JMA model.

The same analysis was also performed for Cu–Cr/Al2O3 sample. Fig. 4 shows the z(α) and y(α) functions for kinetic data. The maximum of z(α) curve, $\alpha_p^{\infty} = 0.394$, was shown by arrow 1. This value is far from the interval $0.62 < \alpha_p^{\infty} < 0.64$ and it could be interpreted that the data does not correspond to the JMA model. However, there is a shoulder that appears in the region shown by arrow 2. This rather complicated shape of the z(α) function can be explained assuming that the nucleation and growth processes partially overlap [38]. As mentioned above, the JMA model is valid provided that all nucleation is completed before the crystal growth started. In the light of these facts, it seems that the nucleation and growth processes probably overlap in the presence Al2O3 nano-particles. This may be explained as follows. Al2O3 nano-particles in Cu–Cr/Al2O3 act as additional and primary nucleation sites compared to Cu–Cr system. It seems that during the growth of pre-nucleated precipitates on Al2O3–Cu interface, secondary nucleation process on the structural defects occurred simultaneously. Therefore, the overall precipitation cannot be described by the JMA model. In this case, the SB empirical kinetic model can be used for a quantitative description of more complicated processes involving both nucleation and growth. The kinetic parameters calculated with Eqs. (9) and (10) are summarized in Table 3. Fig. 1(b) shows the comparison of experimental data (points) and calculated plots (full line) for Cu–Cr/Al2O3 sample. There is relatively good agreement between experimental data and the prediction of SB model. Some discrepancies are observed for this sample at higher temperatures. These discrepancies can probably be caused by different factors. One possibility is the errors in the baseline interpolation for peak tails. Another possible explanation is that the measured data corresponds to a more complex reaction scheme than expressed by SB model. Thermal inertia effects caused by lower thermal contact between the sample and temperature sensor can also play an important role [35].

To compare the ageing behavior of samples in more detail, the DSC curves measured at 5 K/min are shown in Fig. 5, separately. It is evident from the comparison between peaks and onset temperatures that, in presence of Al2O3 reinforcement, the peak is shifted to a lower temperature. Moreover, the ageing is more rapid (sharper peak) in the case of Cu–Cr/Al2O3. As previously mentioned, the higher dislocation density and structural defects as well as Al2O3–Cu interface affect not only the heterogeneous nucleation of precipitates, but also serve as short-circuit paths for diffusion which can accelerate the ageing process. Similar results have been reported in composites of Cu–W [39], Al–SiC [40] and Al–B4C [41].

In order to get a better understanding of the precipitation process and the role of Al2O3 reinforcement, the microstructure of Cu–Cr and Cu–Cr/Al2O3 samples were investigated with TEM. Fig. 6(a) shows the microstructure of Cu–Cr sample after ageing. Fig. 6(b) shows EDS microanalysis performed on dark particles in Fig. 6(a). This confirms that the microstructure consists of fine equiaxed Cu grains and numerous fine Cr precipitates, especially along the grain boundaries. Fig. 6(c) shows the microstructure of Cu–Cr/Al2O3 sample after ageing. Two types of particles can be observed in Cu matrix. EDS microanalysis performed on different regions of 1 and 2 in

Fig. 6(c) confirmed that bright particles are Al2O3 and dark particles are Cr precipitates (Fig. 6(d)). It should be noted that the Cr precipitates closer to Al2O3 are larger than those located inside the copper matrix and along the grain boundaries. It means that the former precipitated prior to the latter. Hence, Al2O3 nano-particles act as the primary nucleation sites and structural defects act as the secondary sites. This confirms the previous explanations about the nucleation and growth overlapping and applicability of SB model for Cu–Cr/Al2O3 sample.

5. Conclusions

The effect of the Al2O3 reinforcement on the ageing kinetic in Cu–Cr solid solution was studied using DSC analysis. Results showed that the presence of reinforcement significantly affects the kinetics of Cr precipitation in Cu matrix nanocomposite. The applicability of JMA model and the SB empirical equation was discussed, as well. The JMA model can be used for description of precipitation process in the case of Cu–Cr sample but the SB model can be applied for the Cu–Cr/Al2O3 sample. It seems that the condition of site saturation was not fulfilled in the case of Cu–Cr/Al2O3 sample and that there is a secondary nucleation process taking place during crystal growth. It was found that the precipitation activation energy decreases in the presence of Al2O3. The presence of Al2O3 accelerates ageing response, primarily due to the higher dislocation density and other structural defects generated during ball milling. Both factors increase the effective diffusivity of Cr and subsequently the rate of the ageing reaction. TEM and EDS analyses suggested that the Al2O3–Cu interface and structural defects act as a primary and secondary nucleation sites, respectively.

Acknowledgments

The support of this work by the Iran Nanotechnology Initiative Council is gratefully acknowledged. The Ministry of Science, Research and Technology of Iran is thanked for funding the first author's sabbatical research in the Instituto de Ciencia de Materiales de Sevilla (CSIC – Universidad de Sevilla). We also thank to the Spanish Government for financial support (Project ENE 2007-67926-C02-01).

References

[1] R.H. Palma, A. Sepúlveda, R. Espinoza, A.P. Zúñiga, M.J. Diánez, J.M. Criado, M.J. Sayagués

High-temperature mechanical behaviour of Cu–Ti–C, Cu–Al and Cu–Ti–Al–C alloys obtained by reaction milling

Mater. Sci. Eng. A, 384 (2004), pp. 262–269

[2] R.H. Palma, A. Sepúlveda, R. Espinoza, M.J. Diánez, J.M. Criado, M.J. Sayagués

High-temperature deformation of dispersion-strengthened Cu–Zr–Ti–C alloys

Mater. Sci. Eng. A, 391 (2005), pp. 60–65

[3] M.T. Márquez, J.B. Correia, J.M. Criado, M.J. Diánez, P. Matteazzi

High temperature stability of a nanostructured Cu–Al2O3 alloy

Key Eng. Mater., 230–232 (2002), pp. 652–655

[4] ASM Metals Handbook

Properties and Selection: Nonferrous Alloys and Special-purpose Materials, vol. 2

Materials Park, ASM International, Ohio, USA (1990)

[5] J.B. Correia, H.A. Davies, C.M. Sellars

Strengthening in rapidly solidified age hardened Cu–Cr and Cu–Cr–Zr alloys

Acta Mater., 45 (1997), pp. 177–190

[6] Y. Jin, K. Adachi, T. Takeuchi, H.G. Suzuki

Ageing characteristics of Cu–Cr in situ composite

J. Mater. Sci., 33 (1998), pp. 1333–1341

[7] N. Gao, E. Huttunen-Saarivirta, T. Tiainen, M. Hemmila

Influence of prior deformation on the age hardening of a phosphorus-containing Cu-0.61 wt.% Cr alloy

Mater. Sci. Eng. A, 342 (2003), pp. 270–278

[8] S. Sheibani, S. Heshmati-Manesh, A. Ataie

Structural investigation on nano-crystalline Cu–Cr supersaturated solid solution prepared by mechanical alloying

J. Alloys Compd., 495 (2010), pp. 59–62

[9] S. Sheibani, S. Heshmati-Manesh, A. Ataie

Influence of Al2O3 nano-particles on solubility extension of Cr in Cu by mechanical alloying

Acta Mater., 58 (2010), pp. 6828–6834

[10] J. Sesták

Thermophysical Properties of Solids. Their Measurements and Theoretical Analysis

Elsevier, Amsterdam (1984)

[11] J. Málek

A computer program for kinetic analysis of non-isothermal thermoanalytical data

Thermochim. Acta, 138 (1989), pp. 337–346

[12] J. Málek

The kinetic analysis of non-isothermal data

Thermochim. Acta, 200 (1992), pp. 257–269

[13] J. Málek

The applicability of Johnson–Mehl–Avrami model in the thermal analysis of the crystallization kinetics of glasses

Thermochim. Acta, 267 (1995), pp. 61–73

[14] G.C. Weatherly, P. Humble, D. Borland

Precipitation in a Cu-0.55 wt.% Cr alloy

Acta Metall., 27 (1979), pp. 1815–1828

[15] M.A. Morris, D.G. Morris

Microstructures and mechanical properties of rapidly solidified Cu–Cr alloys

Acta Metall., 35 (1987), pp. 2511–2522

[16] D.G. Morris, M.A. Morris

Rapid solidification and mechanical alloying techniques applied to Cu–Cr alloys

Mater. Sci. Eng. A, 104 (1988), pp. 201–213

[17] C.P. Luo, U. Dahmen, K.H. Westmacott

Morphology and crystallography of Cr precipitates in a Cu-0.33 wt% Cr alloy

Acta Metall. Mater., 42 (1994), pp. 1923–1932

[18] P. Liu, B.X. Kang, X.G. Cao, J.L. Huang, H.C. Gu

Strengthening mechanisms in a rapidly solidified and aged Cu–Cr alloy

J. Mater. Sci., 35 (2000), pp. 1691–1694

[19] L. Jing-lei, L. Zu-yan, W. Er-de, X. Heng-ze

Structures, properties and responses to heat treatment of deformation processed Cu-15%Cr composite powders prepared by mechanical milling

Trans. Nonferrous Met. Soc. China, 12 (2002), pp. 837–840

[20] H. Wen-xiong, Y. Yang, W. Er-de, S. Hong-fei, H. Lian-xi, C. Hui

Microstructures and properties of cold drawn and annealed submicron crystalline Cu-5%Cr alloy

Trans. Nonferrous Met. Soc. China, 19 (2009), pp. 93–98

[21] M.J. Avrami

Kinetics of phase change. I: general theory

Phys. Chem., 7 (1939), pp. 1103–1112

[22] M.J. Avrami

Kinetics of phase change. II: transformation–time relations for random distribution of nuclei

[23] M.J. Avrami

Kinetics of phase change. III: granulation phase change, and microstructure

Phys. Chem., 9 (1941), pp. 177–184

[24] J. Sesták, G. Berggren

Study of the kinetics of the mechanism of solid-state reactions at increasing temperatures

Thermochim. Acta, 3 (1971), pp. 1–12

[25] V.M. Gorbachev

Some aspects of Šestak's generalized kinetic equation in thermal analysis

J. Therm. Anal., 18 (1980), pp. 193–197

[26] C. Michaelsen, C. Gente, R. Bormann

Phase formation and thermodynamics of unstable Cu–Cr alloys

J. Mater. Res., 12 (1997), pp. 1463–1467

[27] J.M. Criado, A. Ortega

Non-isothermal transformation kinetics: Remarks on the Kissinger method

J. Non-Cryst. Solids, 87 (1986), pp. 302–311

[28] J.M. Criado, A. Ortega

Non isothermal crystallization of metal glasses: simultaneous determination of both the activation energy and the exponent n of the JMA kinetic law

Acta Metall., 35 (1987), pp. 1715–1721

[29] S. Vyazovkin, A.K. Burnham, J.M. Criado, L.A. Pérez-Maqueda, C. Popescu, N. Sbirrazzuoli

ICTAC Kinetics Committee recommendations for performing kinetic computations on thermal analysis data

Thermochim. Acta, 520 (2011), pp. 1–19

[30] A. Varschavsky, E. Donoso

Short-range ordering by excess and thermal vacancies during linear heating experiments in α-Cu–Al alloys

Mater. Sci. Eng. A, 145 (1991), pp. 95–107

[31] M.A. Turchanin

Phase equilibria and thermodynamics of binary copper systems with 3d-metals. iii. Copper–chromium system

Powder Metall. Met. Ceram., 45 (2006), pp. 457–467

[32] J. Szablewski, B. Kuknicka

Activation energy for precipitation in undeformed and deformed Cu–Cr alloys

Phys. Stat. Sol., 108 (1988), pp. K5–K8

[33] D.B. Butrymowicx, J.R. Manning, M.E. Read

Diffusion in copper and copper alloys, part III. Diffusion in systems involving elements of the groups IA, IIA, IIIB, IVB, VB, VIB and VIIB

J. Phys. Chem. Ref. Data, 4 (1975), pp. 177–249

[34] J.J. Hoyt

On the coarsening of precipitates located on grain boundaries and dislocations

Acta Metall., 39 (1991), pp. 2091–2098

[35] J. Málek

Kinetic analysis of crystallization processes in amorphous materials

Thermochim. Acta, 355 (2000), pp. 239–253

[36] D.W. Henderson

Thermal analysis of non-isothermal crystallization kinetics in glass forming liquids

J. Non-Cryst. Solids, 30 (1979), pp. 301–315

[37] D.W. Henderson

Experimental analysis of non-isothermal transformations involving nucleation and growth

J. Therm. Anal., 15 (1979), pp. 325–331

[38] J. Málek, T. Mitsuhashi, J. Ramírez-Castellanos, Y. Matsui

Calorimetric and high-resolution transmission electron microscopy study of nanocrystallization in zirconia gel

J. Mater. Res., 14 (1999), pp. 1834–1843

[39] K.K. Chawla, M. Metzger

Initial dislocation distributions in tungsten fibre–copper composites

J. Mater. Sci., 7 (1972), pp. 34–39

[40] R.J. Arsenault, R.M. Fisher

Microstructure of fiber and particulate SiC in 6061 Al composites

Scr. Metall., 17 (1983), pp. 67–71

[41] T.G. Nieh, R.F. Karlak

Ageing characteristics of B4C-reinforced 6061-aluminum

Scr. Metall., 18 (1984), pp. 25–28

Figure captions

Figure 1. Experimental DSC curves (points) and calculated DSC curves (full lines) of (a) Cu–Cr and (b) Cu–Cr/Al2O3 samples at different heating rates.

Figure 2. XRD patterns of milled and aged (a) Cu–Cr and (b) Cu–Cr/Al2O3.

Figure 3. Normalized (a) z(α) and (b) y(α) functions obtained by transformation of DSC data from Fig. 1 for Cu–Cr sample.

Figure 4. Normalized (a) z(α) and (b) y(α) functions obtained by transformation of DSC data from Fig. 1 for Cu–Cr/Al2O3 sample.

Figure 5. Comparison of DSC curves measured at 5 K/min for Cu–Cr and Cu–Cr/Al2O3.

Figure 6. TEM micrographs of (a) Cu–Cr and (b) Cu–Cr/Al2O3 after ageing. (c) EDS spectra from the zones pointed in (b).

Table 1

Table 1. The most frequently used kinetic models for description of nucleation and growth processes.

Model	**Symbol**	***f*(*α*)**
Johnson–Mehl–Avrami [21], [22] and [23]	JMA	$n(1-\alpha)[-\ln(1-\alpha)]^{1-(1/n)}$
Sestak–Berggren [24] and [25]	SB	$\alpha^{M}(1-\alpha)^{N}$

Table 2

Table 2. Experimental transformation enthalpies and kinetic parameters of Cu–Cr sample (E = 133 ± 5 kJ/mol).

β (K/min)	ΔH (J/g)	n	ln A (A/s^{-1})
5	10.85	1.10	14.86
10	17.96	1.15	14.09
20	17.74	1.21	14.53
40	12.77	1.25	14.19
Average	14.83 ± 3.57	1.18 ± 0.07	14.42 ± 0.35

Table 3

Table 3. Experimental transformation enthalpies and kinetic parameters of Cu–Cr/Al_2O_3 sample (E = 100 ± 3 kJ/mol).

β (K/min)	ΔH (J/g)	M	N	ln A (A/s^{-1})
5	17.26	0.54	1.97	12.29
10	9.94	0.43	1.91	12.21
20	15.74	0.65	1.94	12.68
40	12.19	0.63	1.82	12.65
Average	13.78 ± 3.33	0.56 ± 0.1	1.91 ± 0.06	12.46 ± 0.24

Figure 1

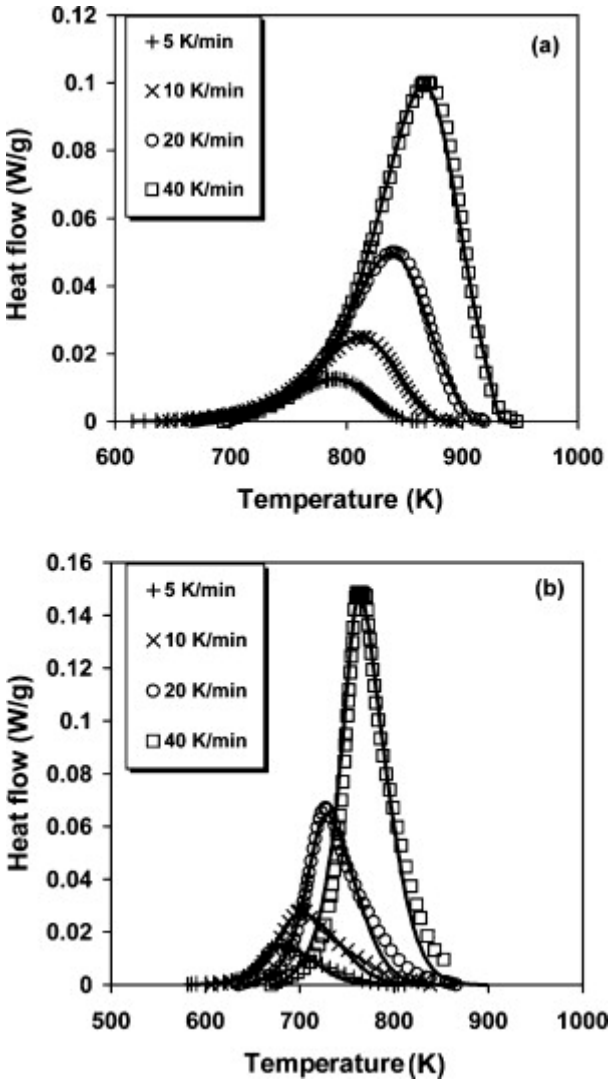
(a)
+ 5 K/min
× 10 K/min
○ 20 K/min
□ 40 K/min
Heat flow (W/g)
Temperature (K)
0.12
0.1
0.08
0.06
0.04
0.02
0
600
700
800
900
1000
(b)
+ 5 K/min
× 10 K/min
○ 20 K/min
□ 40 K/min
Heat flow (W/g)
Temperature (K)
0.16
0.14
0.12
0.1
0.08
0.06
0.04
0.02
0
500
600
700
800
900
1000

Figure 2

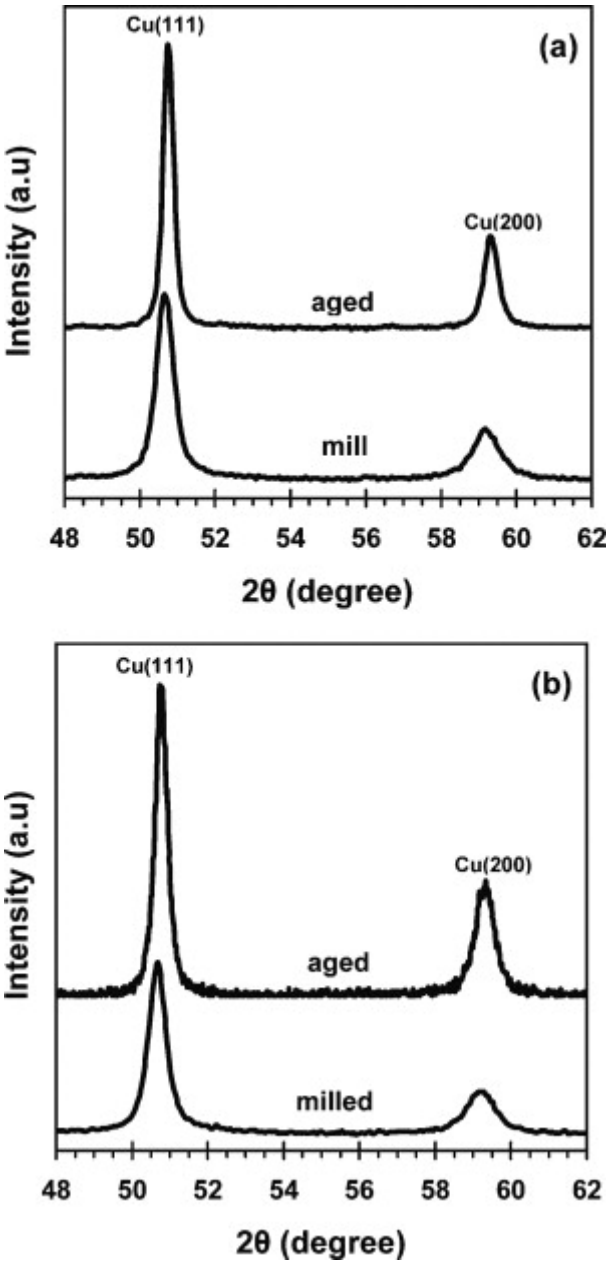
Cu(111)
(a)
Cu(200)
aged
mill
Intensity (a.u)
48
50
52
54
56
58
60
62
2θ (degree)
Cu(111)
(b)
Cu(200)
aged
milled
Intensity (a.u)
48
50
52
54
56
58
60
62
2θ (degree)

Figure 3

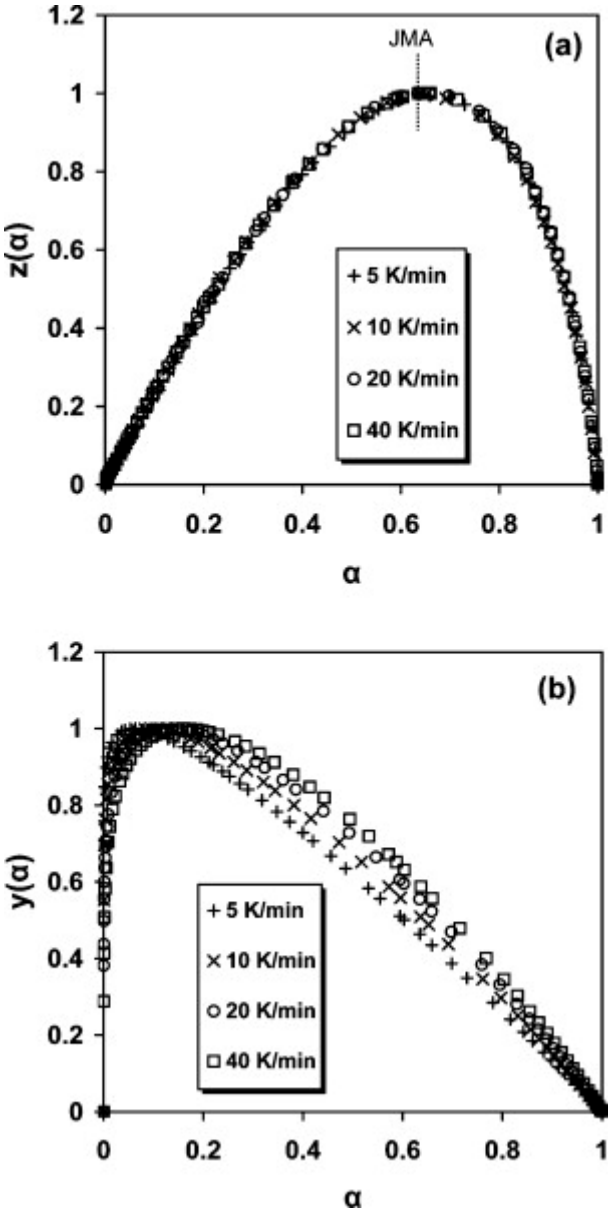
(a)
JMA
z(α)
α
+ 5 K/min
× 10 K/min
○ 20 K/min
□ 40 K/min
(b)
y(α)
α
+ 5 K/min
× 10 K/min
○ 20 K/min
□ 40 K/min

Figure 4

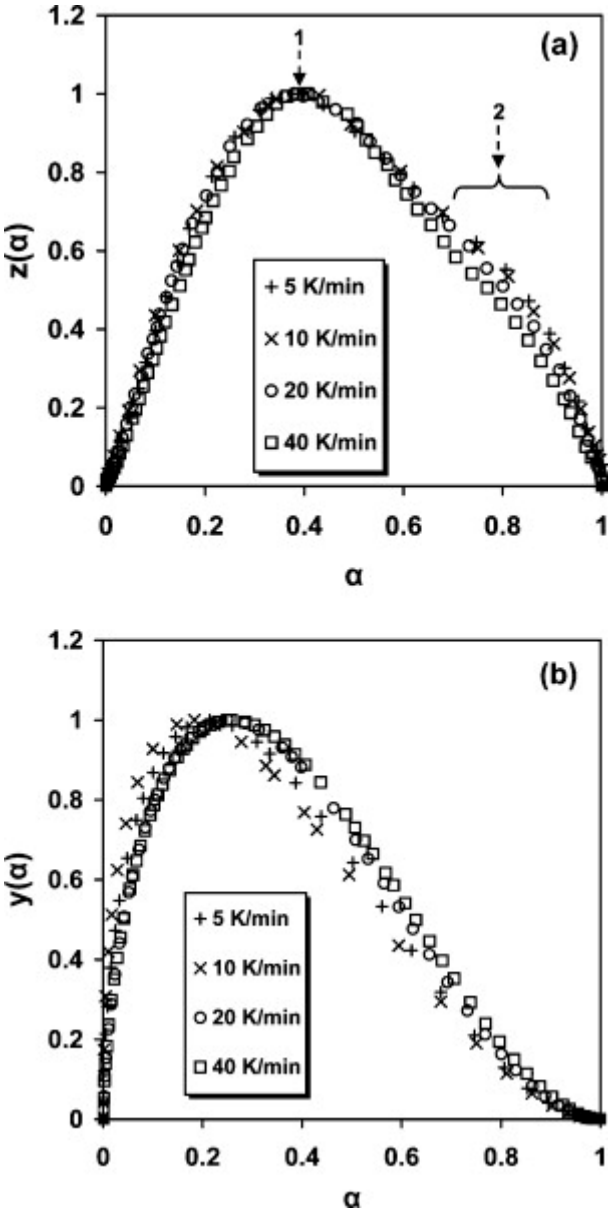
(a)
1
2
z(α)
α
+ 5 K/min
× 10 K/min
○ 20 K/min
□ 40 K/min
(b)
y(α)
α
+ 5 K/min
× 10 K/min
○ 20 K/min
□ 40 K/min

Figure 5

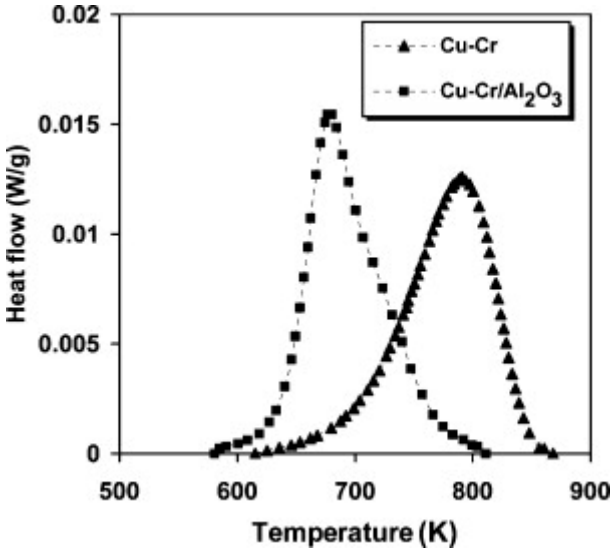
0.02
0.015
0.01
0.005
0
Heat flow (W/g)
500
600
700
800
900
Temperature (K)
Cu-Cr
Cu-Cr/Al2O3

Figure 6

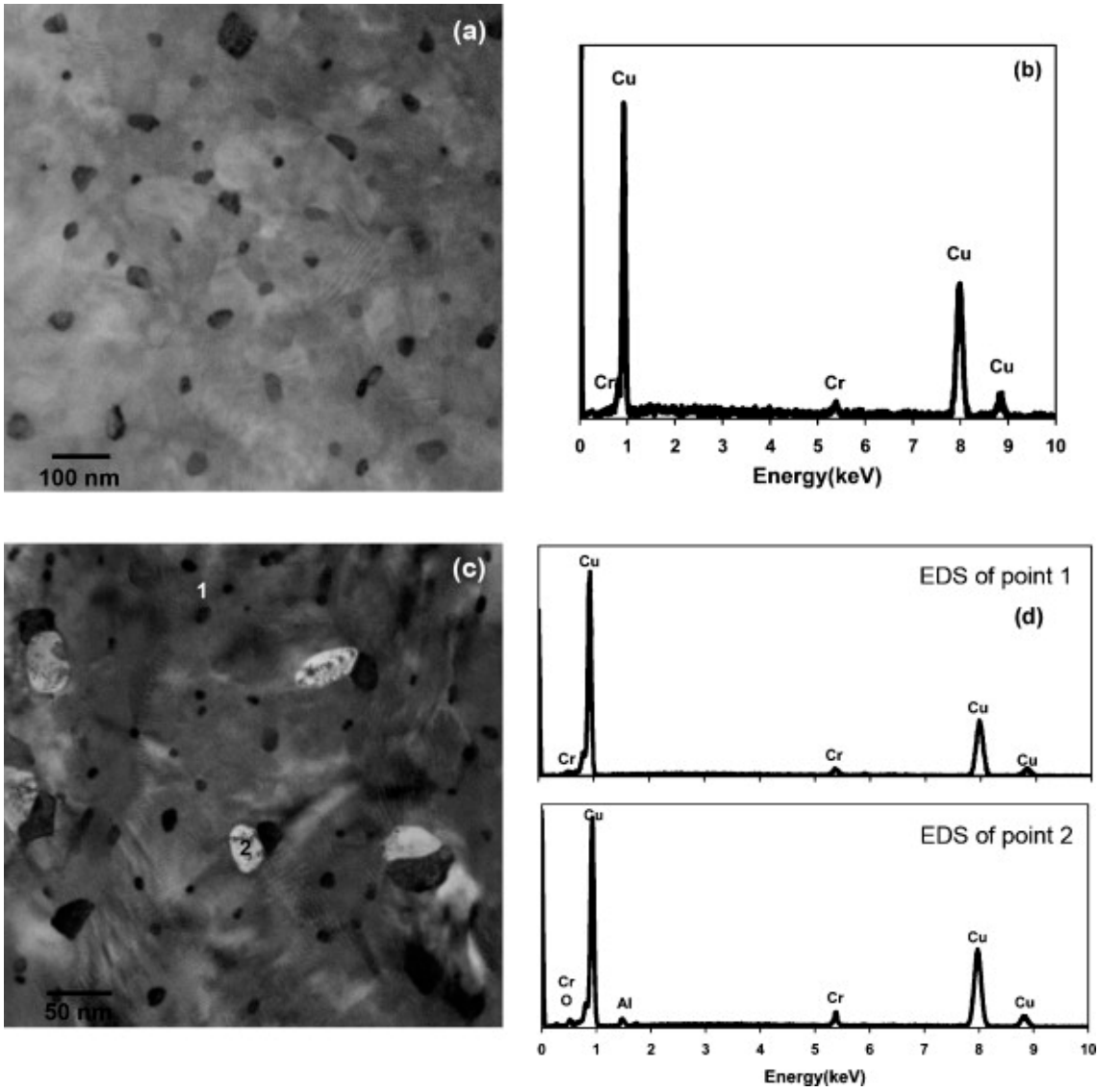
(a)
100 nm
(b)
Cu
Cr
Cr
Cu
Cu
0 1 2 3 4 5 6 7 8 9 10
Energy(keV)
(c)
1
2
50 nm
EDS of point 1
(d)
Cu
Cr
Cr
Cu
Cu
EDS of point 2
Cu
Cr
O
Al
Cr
Cu
Cu
0 1 2 3 4 5 6 7 8 9 10
Energy(keV)